Technical report; TR-249

KNMI

An investigation of the representative heights for atmospheric motion vectors

R. Dlhopolsky and A. Feijt

De Bilt, 2003

Technical Report = Technisch Rapport; TR-249

De Bilt, 2003

PO Box 201, 3730 AE De Bilt
The Netherlands
Wilhelminalaan 10
http://www.knmi.nl
Telephone +31 30 22 06 911
Telefax +31 30 22 10 407

Authors: Dlhopolsky, R.
Feijt. A.

UDC: 551.511.33

ISSN: 0169-1708

ISBN: 90-369-2229-1

An Investigation of the Representative Heights for Atmospheric Motion Vectors

R. Dlhopolsky , A. Feijt

KNMI

The Netherlands

Abstract

The objective of this study is to find out the reason for the biases which exist in the cloud heights of Atmospheric Motion Vectors (AMVs) created by EUMETSAT. A cloud detection and cloud property retrieval tool, referred to as KLAROS (KNMI's Local implementation of APOLLO retrievals in an Operational System), is used to diagnose the biases in the representative heights of the AMVs. The WMO network of radiosondes are used to map the KLAROS cloud temperatures into independent pressures and wind vectors. From a set of 40 NOAA overpasses, an in depth analysis of the cloud fields for 8 NOAA overpasses is performed.

Comparison between the independent wind vectors and the EUMETSAT AMVs lead to the identification of three sources of error. The first is that the semi-transparency flagging for EUMETSAT often occurs under the wrong cloud conditions. The second is that, when the semi-transparency flag is set, the AMV temperatures are weighted too heavily by the water vapor channel brightness temperatures. The resulting cold temperature frequently raises the altitude of the AMVs into a region of maximum wind speed, causing a bias in wind speeds. This depends on the structure of the cloud top boundaries being observed. The third is related to the METEOSAT viewing geometry of the northern latitudes. A consistent temperature difference of 5K was seen between METEOSAT infrared temperatures and nadir viewing AVHRR temperatures for optically thick cloud fields. For clouds traveling at altitudes within the wind shear profile, a bias of 5K can translate into a difference of 30hPa. This implies that the EUMETSAT cloud correction algorithm should be tuned differently for Northern latitudes.

The first source of error can be removed by a re-evaluation of the EUMETSAT criteria for semi-transparency flagging. Removing the semi-transparency correction caused a significant reduction in the wind speed bias for 7 out of the 8 cases. It is suggested that an improved definition of the structure of cloud top boundaries and reinterpretation of the water vapor signal can reduce the second source of error. The effect of viewing geometry on the wind speed bias is related to the second error and has been demonstrated in one case.

Introduction

EUMETSAT Atmospheric Motion Vectors (AMVs) are currently being used in ECMWF models. Results from statistical studies found in the literature show that wind speed biases exist in this dataset (*Bormann, N.*, 2001). In order for this data to be assimilated into the ECMWF environment, the bias must be removed. It is suspected that these biases are related to the height assignment of tracked clouds.

The objective of this study is to find out if the biases which exist in the wind vectors can be attributed to the representative cloud heights of the AMVs and to find a physical explanation which can be used to improve the AMV product. Results are an abridged version of research done for EUMETSAT, (*Dlhopolsky and Feijt*, 2003). A cloud detection and cloud property retrieval tool, referred to as KLAROS (KNMI's Local implementation of APOLLO retrievals in an Operational System), is used to estimate an accurate cloud top temperature. Data from the WMO network of radiosondes are used to map the KLAROS cloud top temperatures into independent vertical pressures and wind vectors. Verification of cloud height and structure is done with a ground radar located in Delft. From a set of 40 NOAA overpasses, an in depth analysis of 8 NOAA overpasses is performed. These cloud fields were chosen explicitly for their cold temperatures and wide range of KLAROS estimated emissivities, from opaque to semi-transparent.

Method

In this section, we describe the geographic area of investigation, criteria for selecting the days to study, satellite data and the satellite product data.

The area of study is centered over the Netherlands and includes Belgium, northern Germany and the North Sea. Figure 1 shows the area viewed by the NOAA-AVHRR instrument and the radiosonde station locations. Note that this is within the accepted 55° boundaries for creation of AMVs from METEOSAT data.

Dates for the study were chosen from the database of the CLouds and Radiation project, CLARA, (*Feijt et al., 1999*). The criteria for selection of cases was high variability in the cloud optical thickness and cold temperatures (less than 250K). Out of 40 experiment days, eight were selected for detailed analysis.

Cloud clusters of AVHRR pixels are defined for each AMV region, with an area of $\pm$ 0.25° in longitude and latitude. This includes roughly 45 x 45 AVHRR pixels, depending on the viewing angle of the AVHRR instrument.

Instrument Data

The surface location of the radiosondes used are shown in Figure 1. Locations on subsequent figures are identified by the first letter of the station except for Essen, where it is assigned an S. Noon radiosondes are used. The time between the sounding and the AVHRR satellite overpass is not longer then an hour. Co-location in space is made at the ground and some error is introduced which is due to the travel of the radiosonde away from these coordinates.

The cloud top boundaries of the clouds over Delft are described with the use of ground based 3.315GHz radar measurements collected during the CLARA project. This data is in the form of a time series of measurements above one location and give a good representation of temporal variation of the vertical dimension of the cloud field.

NOAA-14 AVHRR afternoon images are used. The spatial resolution is about 1.1km at nadir and 8km near the terminator. Calibration is performed according to the standard NOAA calibration recommendations (See (*Rao and Chen*, 1996)). Calibration is a major source of inaccuracy in reflectivity measured from the NOAA-AVHRR instruments. The reflectivities from channel 1 (0.58-0.68μm) are normalized to overhead sun.

Brightness temperature measured by METEOSAT-7, wvT (5.7 - 7.1μm) and irT (10.5 - 12.5μm) will be used for comparison. METEOSAT-7 views Northern Europe with a viewing angle of about 50° to 65°. Images with the nearest half hour to the NOAA overpass were used in this study.

Product Data

Product data is defined here as a description of data which has been created from the combination of instruments, tracking software and radiative transfer models. The software which does this is called the analysis environment. We discuss two analysis environments: EUMETSAT and KNMI KLAROS.

EUMETSAT estimates cloud heights for a 16x16 pixel cluster of clouds within an AMV region based on three conditions: semi-transparency, opaque clouds and 30% cloudiness. In the EUMETSAT semi-transparency correction scheme, the cloud heights are derived using $H_2O - IR$ intercept method (*Schmetz, J., et al., 1993*).

The EUMETSAT AMVs are generated with the use of a sophisticated cloud tracking algorithm with automatically generated quality control factors. The method seeks out gradients in infrared radiances and correlates the pattern over three time slots. The target size for the AMV database used in this study is 16*16 METEOSAT pixels. This is a higher resolution prototype for future use with the MSG satellite data. Each target will be referred to

as an AMV region.

In addition to the wind vectors, the EUMETSAT AMVs contain a set of quality indicators, QI, which are a measure of the confidence in the accuracy of the vectors. The weighting functions for calculating the quality indicators are: consistency in time with respect to speed, direction, vector , spatial consistency and consistency with a forecast wind field (*Holmlund, K.*, 1998).

A comparison data set is supplied by the cloud property retrieval environment at KNMI. A combination of NOAA AVHRR satellite data and radiative transfer (RT) modelling produce the cloud products, cloud top temperature, T_{cloud}, and cloud infrared emissivity, ϵ_{ir}. We refer to products of this environment with the acronym KLAROS (KNMI Local implementation of APOLLO retrievals in an Operational System). KLAROS operates on individual pixels. Optical thickness is determined using RT models to associate a visible reflectivity with a visible optical depth, τ_{vis}. After some assumptions about crystal characteristics, an ϵ_{ir} can be estimated. A cloud top temperature, T_{cloud}, is estimated from this emissivity and ground temperatures. Since most of the pixels for images used in this study are cloud contaminated, ground temperatures are set by the High Resolution Limited Area Model, HIRLAM (*Gustafsson, N.*, 1993).

Emissivity of 1 will indicate an opaque cloud and T_{cloud} will be equal to the AVHRR 10.8μm brightness temperature. KLAROS also contains a detection capability for semi-transparent clouds based on the AVHRR 10.8μm and 12.0μm channels. Thresholds for this detection are defined by (*Saunders and Kriebel*, 1988). The vegetation signal, 0.8μm 0.6μm, is used to qualitatively estimate semi-transparency. However, it is the cloud ϵ_{ir} and the difference between the 10.8μm temperature and the surface temperature which determines the corrected cloud top height.

Results

The case studies were selected based on variability of the cloud field with respect to τ_{vis} and T_{cloud}. It was expected that large variability would lead to large height assignment errors and that these could be investigated with the high resolution KLAROS cloud properties. We looked closely at the relationship between the height differences and wind speeds by overlaying the AMV wind speeds for regions with $QI \geq 80\%$ onto the radiosonde profiles. A consistent pattern in the differences between the heights of the KLAROS and AMVs was found for all the cases. The AMV cloud top heights were always higher than those of KLAROS. In addition, regardless of degree of cloudiness, all of the AMVs were assigned cloud top heights with the semi-

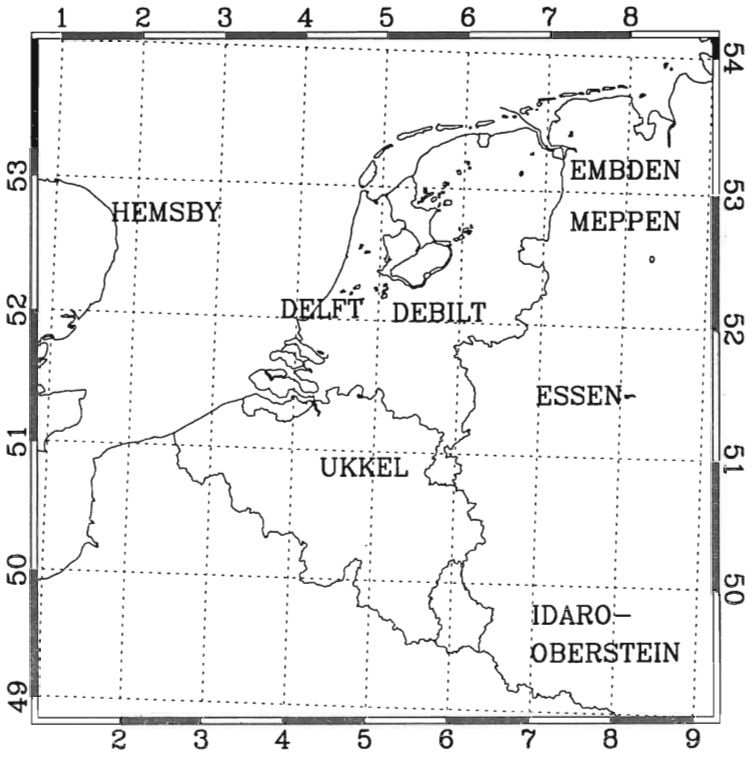

Figure 1: Radiosondes within the area viewed by AVHRR satellite image. Note that S represents Essen in all figures.

transparency method. The following sections present details of these results for each case.

Case Studies

In this section we show results from each of the selected case studies. The AMVs are plotted in Figure 2 and 4. The vectors overlay a photo-negative image of the AVHRR 10.8 micron temperatures. The figures with the vertical wind speed profiles are shown in Figure 3 and Figure 5. Letters refer to the radiosonde stations shown in Figure 1.

17 April, 1996

The cloud field on this day is a front crossing the Netherlands from the SW heading NE, the direction of motion of the field is approximately 225°. There

is considerable variability in the wind direction of the clouds at the edge of this cloud field. Figure 2 (a) shows that most of the vectors with $QI \geq 80\%$ lie in the north of the image. Figure 3 (a) shows that the average height differences between AMV and KLAROS are greater than 75hPa. There is considerable variability in the KLAROS pressure heights, even though most of the regions contain optically thick clouds (only 2 were corrected for semi-transparency). The AMV wind speeds match the radiosonde wind speeds at the KLAROS cloud heights better than at the AMV cloud heights.

24 August, 1996

The cloud field for this day shows developing clouds moving along with the atmospheric flow, in a north easterly direction (225 degrees). Figure 2 (b) shows that there are many vectors, a majority of which have a $QI \geq 80\%$. Figure 3 (b) shows that the wind speed is nearly constant with altitude, except for stations in the east of the image. Differences in wind speed between the two methods are difficult to quantify in this case since there is no variability in wind speed with height. Nevertheless, the AMV pressure heights are clustered around 300hPa and differ by 100hPa from the associated KLAROS pressure heights. The cloud field is strongly affected by semi-transparent effects at the cloud edges and optically thick clouds at lower altitudes (higher pressures).

28 August, 1996 12:24, 14:06

The cloud field for this day is the northern part of a cyclonic system. Above 500hPa, most of the radiosondes have a wind direction SSE. On this day, the NOAA satellite viewed the Netherlands from two different orbits. The vectors for both plots in Figure 2 (c) and (d) are from the same AMV data set. This cloud field was more difficult for the tracking software, and resulted in a smaller number of high quality AMVs. The general motion of the system seems to be captured well, regardless of the quality factors. The low quality is related to the QI consistency in direction which has large deviations near the center of a low pressure area. Note that the underlying AVHRR image applies to the different orbits.

Figure 3 (c) shows that the magnitude of the difference in pressures from the two methods varies, but always the KLAROS pressures are at lower altitudes than the AMV pressures. The height of the AMVs is located within the section of the atmosphere with the largest wind speed. If the wind speed is too slow, the error is in the tracking. If the cloud height is too high, the error is in the height assignment. The selection of only high quality vectors

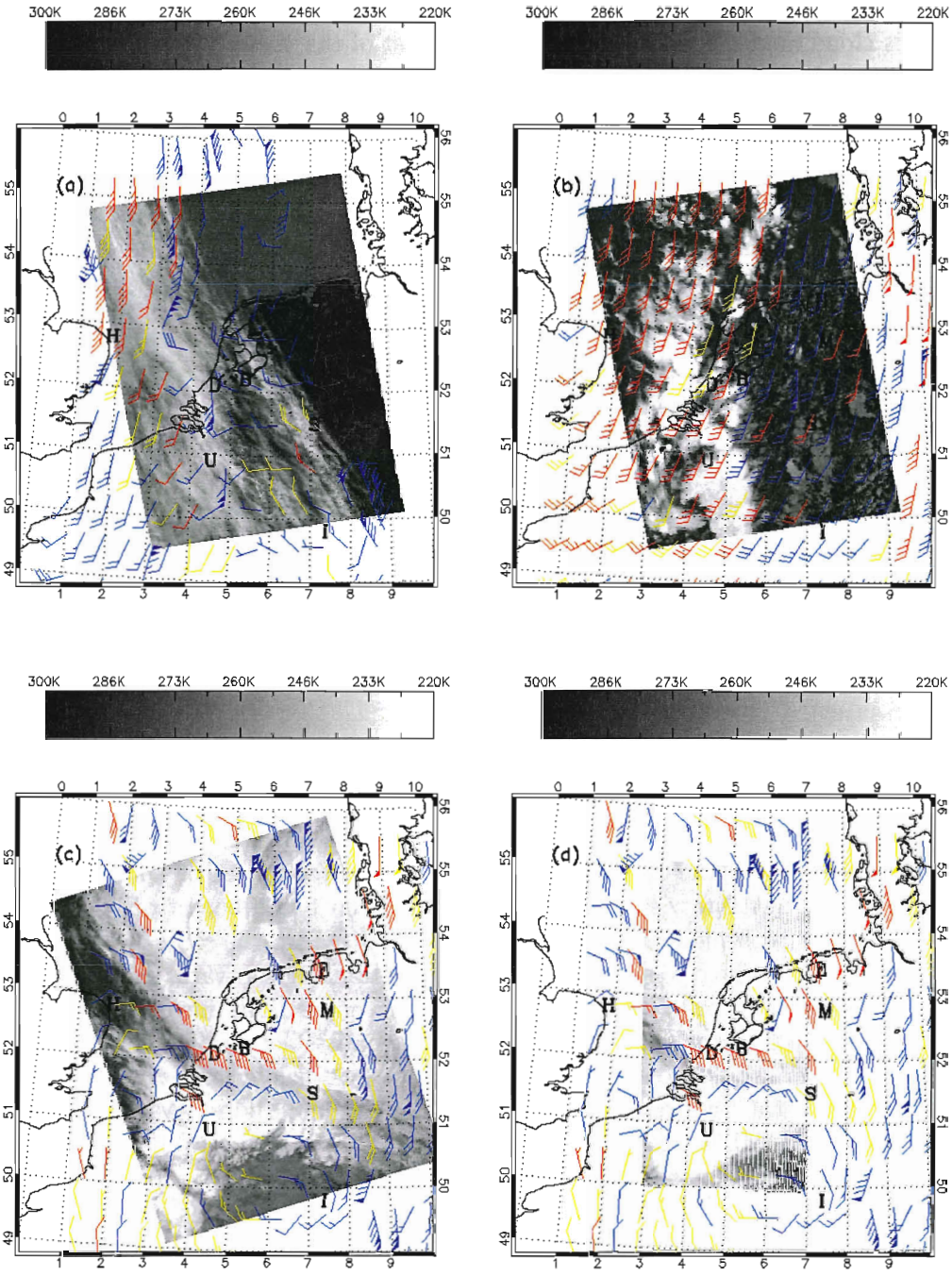

Figure 2: (a) 17 April 13:02, (b) 24 August 13:08, (c) 28 August 12:24 (d) 28 August 14:06; Wind Vectors, Red = $QI \geq .8$, Yellow = $0.6 \leq QI < .8$,Blue $QI < .6$.

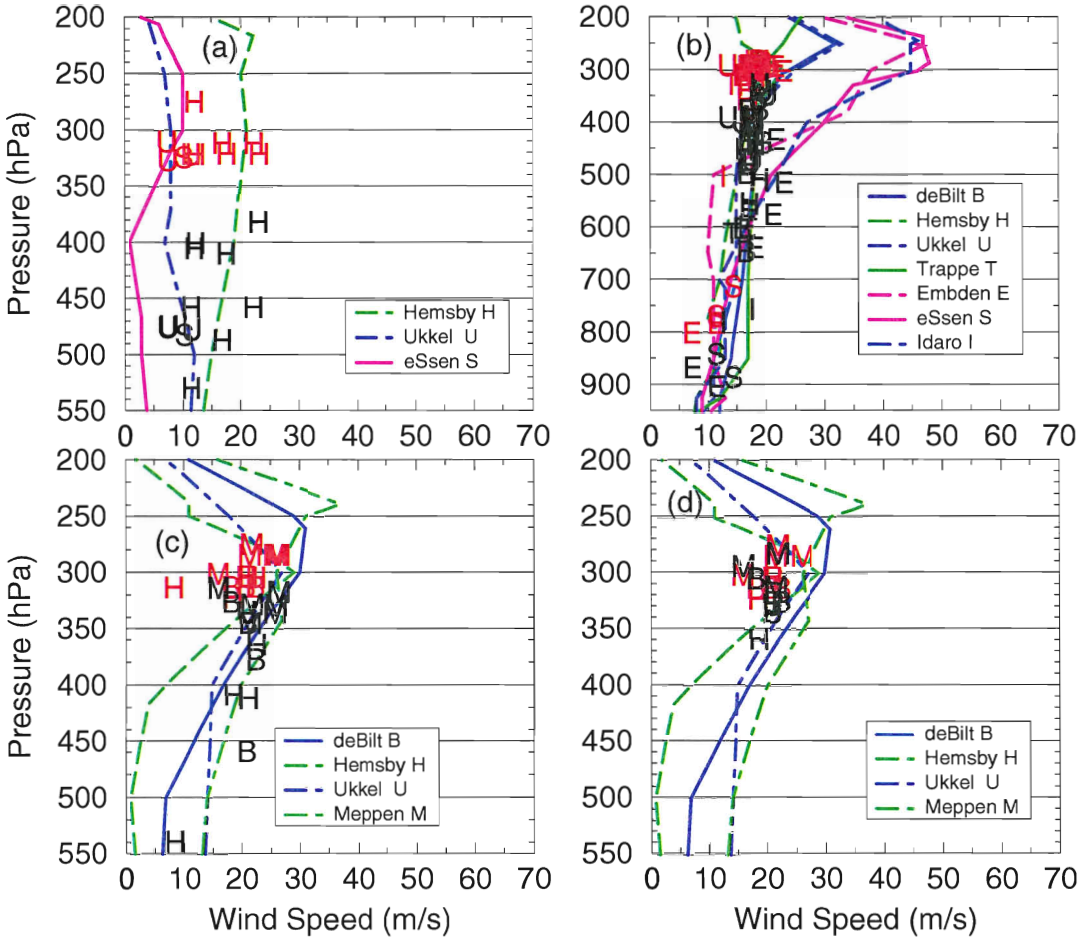

Figure 3: Wind speed profiles for (a) 17 April, (b) 24 August, (c) 28 August (first orbit), (d) 28 August (second orbit). Black letters refer to KLAROS cloud heights, Red letters refer to AMV cloud heights.

supports the second interpretation of the results.

In Figure 3 (d), the difference between the AMV and KLAROS pressures is smaller. This suggests that, either the cloud tops are colder for the second orbit (a valid interpretation if the radar images over Delft are representative of the enitre cloud field over the Netherlands (See Figure 8 (middle)). Another possibility is that there is a viewing angle dependence on the cloud top temperature determination. All of the high quality AMV regions are optically thick for both orbits. If the first AVHRR image can be considered the beginning image for the cloud tracking, and the second could be considered the last image for the cloud tracking, this is an example of the difficulties in assigning a cloud height to a cloud field which is changing over 1.5 hours.

18 November, 1996

Figure 4 (c) shows two distinct cloud fields within a cylonic system. One is located over the NW corner of the image and is warm, with a T_{cloud} of about 250K. The second, also part of a cyclonic system, consists of much colder cloud tops. The wind vectors with QI >80% are all associated with the coldest part of the cloud field. The fact that these AMVs are clustered gives more confidence that they are correct. Figure 5 (a) shows a consistent difference between the AMV pressure heights and KLAROS pressure heights of about 50hPa. All of these regions are optically thick. These results are similar to those of 28 August, which also had a prominent wind speed gradient near 300hPa.

24 November, 1996

The cloud field on this day is approaching the Netherlands from the W, NW (300 degrees). The cloud top temperature of the approaching cloud is between 225K and 240K, average about 235K. There is a lower altitude cloud field in the eastern part of this image (right side) with a temperature between 240K and 275K, average about 265K. Most of the high QI vectors in Figure 4 (b)) appear in the colder cloud field. The wind speed profiles in Figure 5 (b) show two effects. The strong wind speeds to the right of the profile are associated with cloud clusters which posed a problem for cloud height determination for both the AMVs and KLAROS, although the wind speed determined from the tracking seems accurate. The cluster of AMV regions around 275hPa, excluding those with the height problem, is lower in pressure by 50hPa, compared with the KLAROS pressures. As in the cases for 28 August and 18 November, the location of the pressure heights within the high wind speed gradient makes the wind speeds appear slower.

27 November, 1996

The cloud field on this day consists of several cloud fields, one at the center of the image is not moving, the ones in the north and south are moving in opposite directions with respect to each other. The north cloud field is made up of broken clouds, as shown in Figure 4 (c). This field is moving west. There is a frontal system at the bottom of the image moving east. The broken clouds in the north have T_{cloud} around 260K. The temperature of the cloud field from the west is about 240K. Between these two systems are two smaller cloud fields, one near the Netherlands coast with $T_{cloud} = 257$K. The AMV generating environment had difficulty with these cloud fields, as demonstrated by the lack of vectors with high quality. The KLAROS pressure heights around Embden, Figure 5 (c), are affected by the broken cloud structure. The single point at Ukkel is interesting because both the AVHRR and METEOSAT irT match for this region. The METEOSAT wvT in this instance appears to give a cloud height which matches the assigned speed. This is however, only one data point.

3 December, 1996

The cloud field for this day is approaching the Netherlands from the West (270 degrees). Figure 4 (d) shows that there are not many high quality AMVs for this day. The homogeneity of the cloud field seems to have posed some difficulty for the cloud tracking algorithms. A greater number of high quality vectors are located in regions with large temperature variability. This temperature variability makes it difficult to assign one height to the vectors. The temperature range of the cloud from west to east in the center of the image is between 225K to 230K, that in the top and bottom of the image is between 245K and 260K.

Figure 5 (d) shows a wide range of wind speeds. The KLAROS pressure heights are consistently at higher pressures (lower altitudes) than the AMVs, although the magnitude of the difference varies.

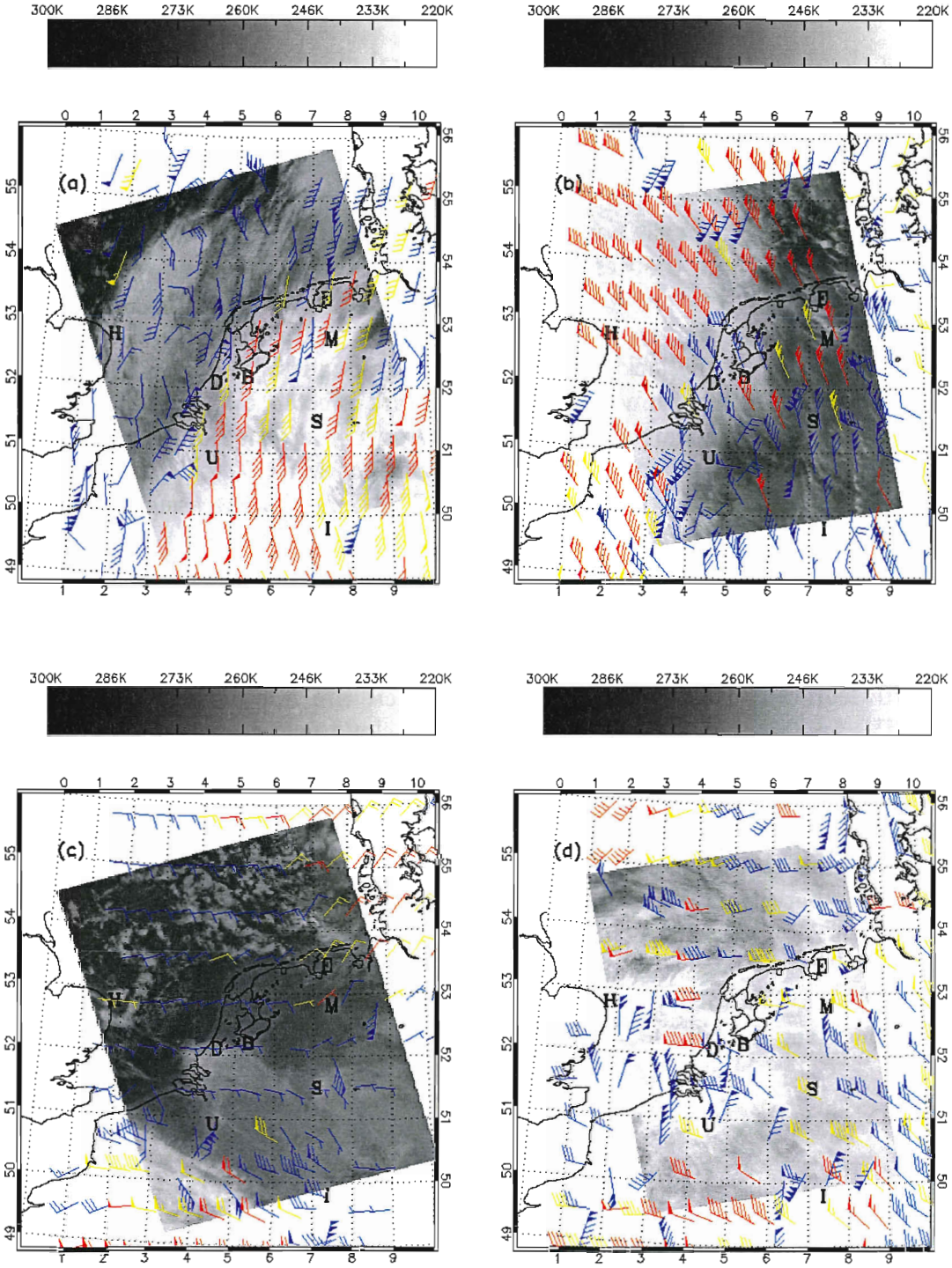

Figure 4: (a) 18 November, (b) 24 November, (c) 27 November, (d) 3 December Wind Vectors, Red = $QI \geq .8$, Yellow = $0.6 \leq QI < .8$, Blue $QI < .6$.

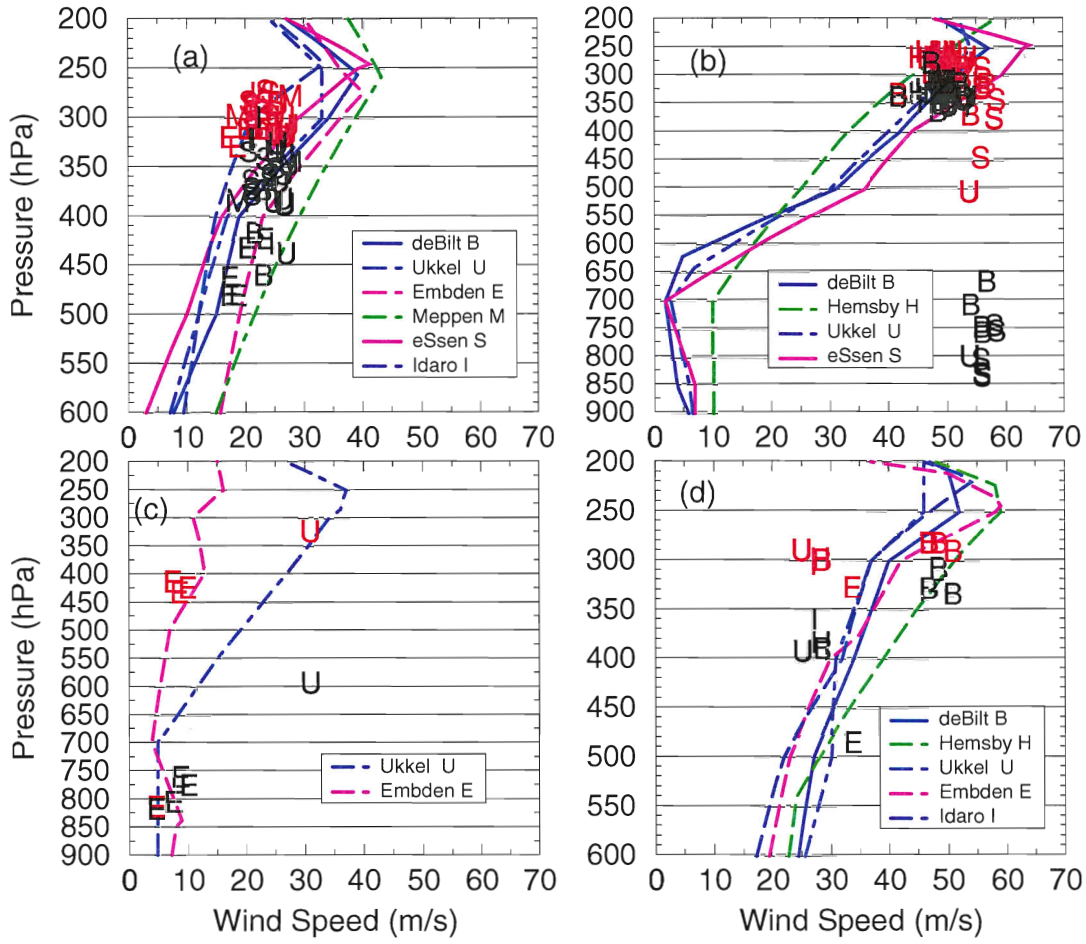

Figure 5: Wind speed profiles for (a) 18 November , (b) 24 November, (c) 27 November , and (d) 3 December. Black letters refer to KLAROS cloud heights, Red letters refer to AMV cloud heights.

Discussion

The results show a consistent difference between the heights of the AMVs and the KLAROS cloud top heights of about 50hPa and greater. A slow wind speed bias appears because of the location of these lower AMV pressure heights within a region of high wind shear. Results of the in depth study of these differences, (*Dlhopolsky and Feijt*, 2003), pointed to three factors which contribute to the cloud height differences which cause the wind biases:

- EUMETSAT semi-transparency flags for the AMV cloud clusters occur more often than would be expected based on the KLAROS cloud temperatures and emissivities.
- The EUMETSAT semi-transparency correction causes a bias towards cold temperatures which is due to the influence of the temperatures estimated from the METEOSAT water vapor channel, wvT. In cases with strong wind speed gradients, the temperature bias corresponds to a wind speed bias.
- On average, for cloudy regions, METEOSAT infrared temperatures, irT, are colder than the AVHRR 10.8μm temperatures by 5K.

The first factor refers to the types of cloud fields (clusters of pixels) defined in the AMV data set: semi-transparent clouds, opaque clouds, and partially filled cloud fields. Each cluster of pixels around an AMV region is assigned a flag which determines how the cloud top temperature is determined. An opaque flag means that the actual irT will be used as the representative height. The 30% flag means that roughly 30% of the pixels are opaque and the temperature is assigned to that of the opaque pixels. The semi-transparency flag means that there is surface interference in irT. When this flag is assigned to a cluster, it means that the cloud top temperature has been estimated using the water vapour- infrared regression technique.

Table 1 shows the sampling of each of the cloud flags for the high quality (80 %) AMV regions in this study. In addition, the average KLAROS cloud emissivity, $\bar{\epsilon}$, for these regions is listed in the last column. The emissivity can be interpreted in this context as a measure of the surface interference in the measured temperatures. We conclude from Table 1, that for 28 August, 18 November and 3 December, the semi-transparency flags are incorrectly assigned.

Figure 6 shows the average temperature correction for the high quality AMV regions. Note that the pattern from case to case is followed closely, although the magnitudes of the corrections differ. For the cases 28 August, 18

Table 1: Number of AMV regions for each flag of cloud cluster analysis with quality factor greater than 80%. Value in parentheses is flag for all QI. $\bar{\epsilon}$ is average KLAROS emissivity.

Date	Semi-transparency	Opaque	30%	$\bar{\epsilon}$
17 Apr 13:02	15 (88)	0 (3)	0 (14)	0.85
24 Aug 13:08	52 (107)	0 (1)	4 (5)	0.69
28 Aug 12:24	14 (112)	0	0	0.98
28 Aug 14:06	9 (58)	0	0	0.99
18 Nov 12:36	35 (128)	0	0	1.00
24 Nov 13:11	47 (107)	0 (1)	0 (4)	0.86
27 Nov 12:39	6 (123)	1 (2)	0 (2)	0.69
03 Dec 13:14	14 (90)	0	0	0.99

November and 3 December, the temperature correction is 5K when there has been only a small amount of correction for KLAROS (assuming cloud tops made of ice particles). For the other cases, the AMV temperature corrections are twice as strong as those for KLAROS (ice).

The second factor, is related to the first. For cases where the semi-transparency flag is set, the height of the clouds within the AMV region is estimated by a regression between the infrared radiances and the water vapor radiances. Figure 7 shows the average temperatures of cloudy pixels within the AMV regions. The average includes opaque and semi-transparent pixels; clear pixels have been removed within the KLAROS analysis environment. The combined opaque and uncorrected, semi-transparent pixels are represented by the AVHRR (10.8 μm) and irT curves (Met IR). For the cases 28 August, 18 November and 3 December, KLAROS and AVHRR 10.8 μm are equal. For these cases, the difference between the AMV cloud top temperature and the METEOSAT wvT is about 2K. The difference betwween the AMV cloud top temperature and METEOSAT irT temperature is about 5K. The similarity between the AMV cloud top temperatures and the METEOSAT wvT is very strong for most of the cases. We conclude from this analysis that the reason the temperature corrections are stronger is related to the use of the METEOSAT water vapor channel in the regression scheme. The water vapor channel is detecting evidence of cloud at these cold temperatures. The question remains, however, is the speed of the cloud cluster correct at these heights?

We show in Table 2 that the wind speed bias can be interpreted as being caused by the height assignements. The altitude at which the AMV cloud

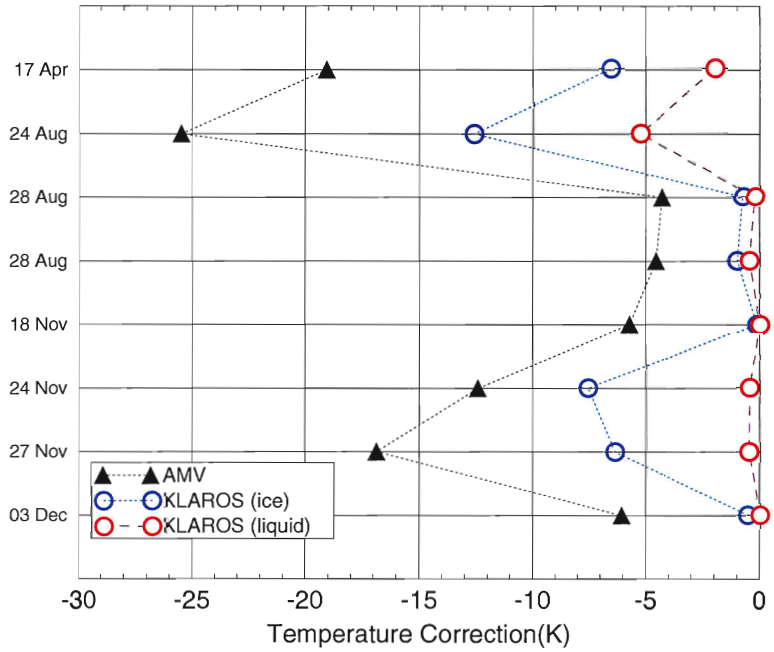

Figure 6: $\overline{\Delta T}_{AMV}$ and $\overline{\Delta T}_{KLAROS}$ (ice and liquid DAK) for each case.

Table 2: Wind speed bias, ΔWS is the difference between the wind speed and radiosonde wind speed at a pressure level defined by the temperature. Values listed are averages of all ΔWS for 80% AMV regions.

Date	N	$\overline{\Delta WS}_{AMV}$ (m/s)	$\overline{\Delta WS}_{KLAROS}$ (m/s)	$\overline{\Delta WS}_{irT}$ (m/s)
17 Apr 13:02	15	-3.2	-1.0	-0.3
24 Aug 13:08	52	-8.3	1.6	2.6
28 Aug 12:24	14	-5.3	1.6	0.1
28 Aug 14:06	9	-7.0	-2.8	-3.9
18 Nov 12:36	35	-7.0	2.1	-2.2
24 Nov 13:11	47	1.0	14.8	14.4
27 Nov 12:39	7	-2.3	1.9	2.6
03 Dec 13:14	14	-9.6	-2.4	-5.6

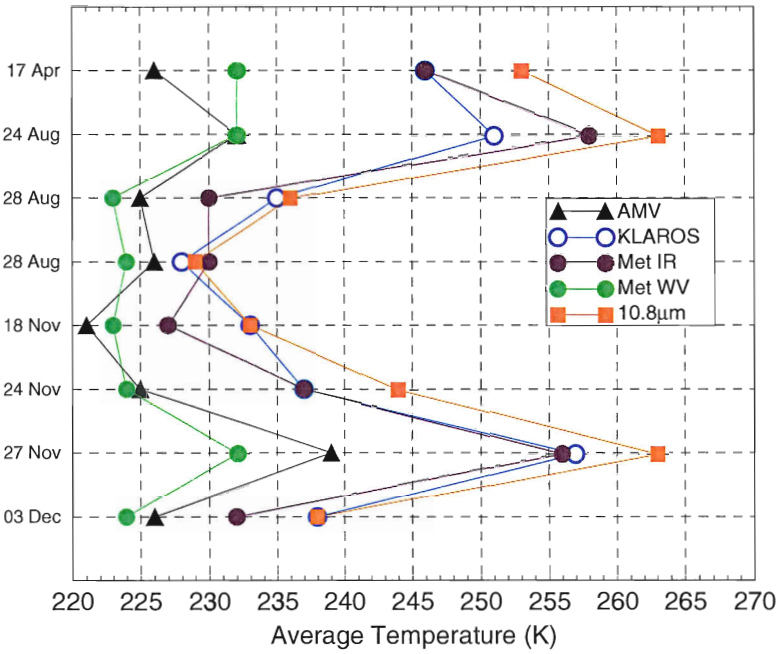

Figure 7: AMV temperatures and average temperatures of KLAROS, METEOSAT IR and WV, AVHRR 10.8 μm.

top temperatures are located, when compared with a radiosonde, result in a wind speed bias which is negative for 7 out of the 8 cases, with a range of -2 to -10 m/s. The altitude at which KLAROS assigns the cloud tops, on the other hand, have wind speed biases which are less than $\pm$ 3 m/s for all but one of the cases. The altitude at which the cloud tops would be assigned if there was no semi-transparency correction (as described above), is shown in the third column, for irT. The wind speed bias is smallest for the wind speeds at KLAROS average cloud top temperatures. This suggests that the temperature corrections are causing the wind speed bias.

The only case which shows almost no wind speed bias is 24 November. Some of the AMV regions for this cloud field consisted partially of pixels which measured cold cloud wisps which were well tracked by the AMV. Within the same AMV regions were breaks in these clouds where a warmer cloud field near the surface was detected by the METEOSAT and AVHRR infrared sensors. This caused the average infrared temperatures to be warmer than the tracked cloud. The water vapor temperatures were effective in identifying the height of the tracked cloud cluster, since the water vapor sensor cannot detect a cloud signal below 600hPa.

The third factor in the cloud height estimation is the observation that, on average, for cloudy regions, METEOSAT irT are colder than the AVHRR 10.8μ m temperatures by 5K. This can be seen in Figure 7 for cases where the AVHRR 10.8 μm and the KLAROS average temperatures overlap, 28 August (first orbit), 18 November and 3 December. The case of 28 August, the second orbit, is the only case where the average temperatures nearly overlap. METEOSAT views the mid-latitudes at an angle of roughly 50°. The 14:06 UTC orbital overpass views the Netherlands also at an angle of roughly 50°. It is the only case where the temperature differences are less than 5K. This implies that the EUMETSAT cloud correction algorithm should be tuned differently for regions which are viewed at large viewing angles.

In order for the wind speed bias to be effectively removed, there must be an explanation for why this is occurring. A clue can be found in the Delft radar images shown in Figure 8. These images show variation of cloud properties in the vertical dimension as the cloud field drifts over Delft. The radar image for 27 November over Delft is shown in the top of Figure 8. The radar images measured on 28 August and 3 December are shown in the middle and bottom, respectively. The cloud top boundarires of the last two are quite different from the first Figure 8. These images demonstrate two distinct types of cloud top boundaries. Figure 8 (top) is an example of a sharp cloud boundary and there is little uncertainty as to the definition of

the cloud top. However, the estimation of the cloud top from the diffuse edges seen in the last two figures in Figure 8 is more uncertain. Based on the these signals, the water vapor channel is probably detecting the higher altitude, diffuse part of the cloud. The ice particle density may not be large enough to affect the infrared channel. This suggests a link between the type of cloud top boundary and the wind speed bias.

The cloud tops in the last two radar images of Figure 8 are not uncommon at the latitudes of the Netherlands. A global survey of cloud top heights measured by a limb-observing satellite, SAGE II, showed that at mid-latitudes, there is an equal distribution of sharp and diffuse cloud tops (*Liao, X., et al.*, 1995). A limb viewing satellite is better able to detect thin clouds at higher altitudes.

Therefore, our concept of the observations is that the tops of the clouds are diffuse and well detected by the water vapor channel. This layer, however, is too "sparse" to significantly affect the infrared radiances. The AMV height assignment processing defines the cloud top to be at the diffuse edge (the level where the first cloud particles occur). The METEOSAT infrared channel that is used to do the cloud tracking is not sensitive to this layer and measures, instead, temperatures at the "sharp edge", which is located lower in the atmosphere (or deeper into the cloud). For these cases, the "surface" over which the semi-transparent cloud lies is actually the sharp edge detected by the infrared sensors.

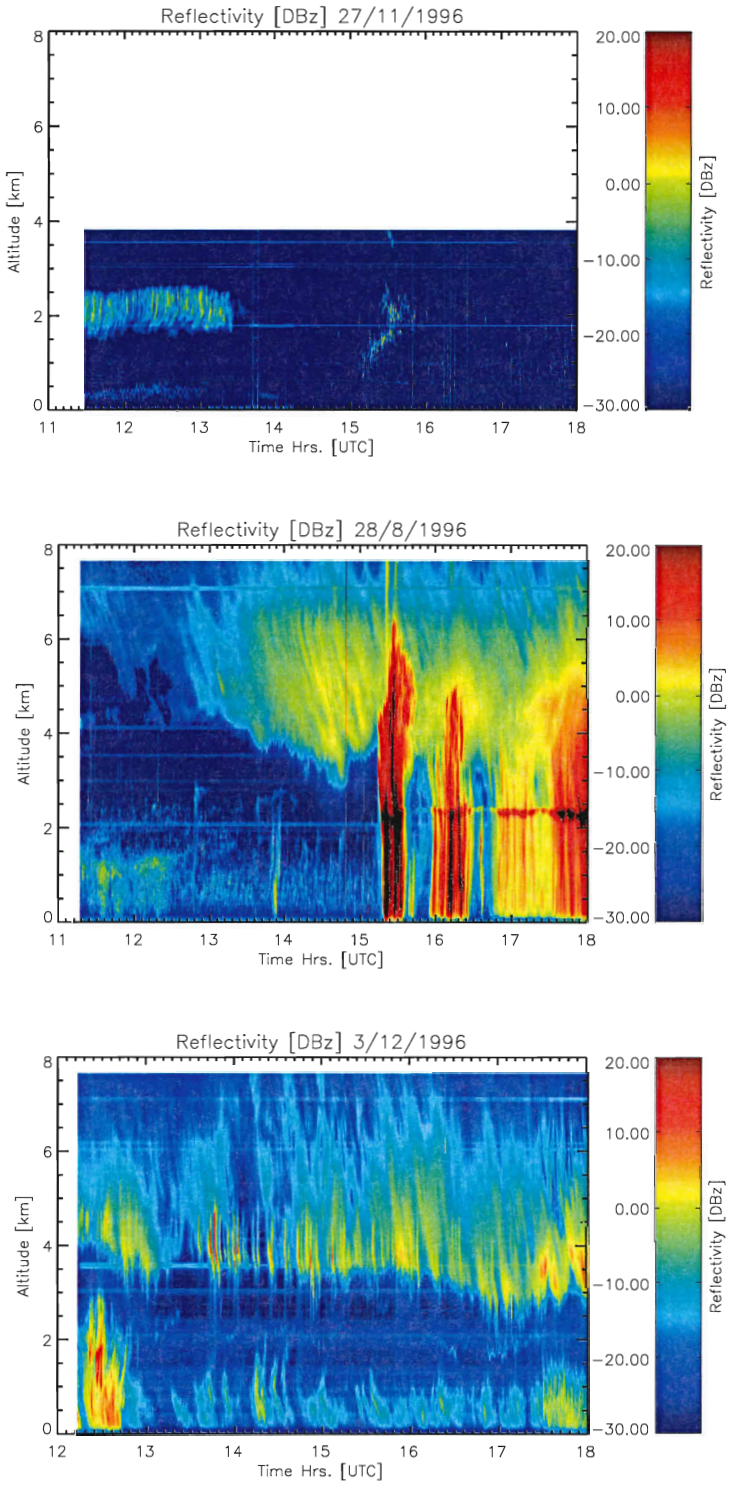

Figure 8: 27 November, (top), 28 August, (middle), 3 December, (bottom) (Source: CLARA, Clouds and Radiation Experiment, 1996).

Conclusion

In conclusion, we have verified that there is a temperature bias in the AMV cloud heights and have shown that this causes the altitude of the atmospheric motion vectors to be assigned to an altitude where the radiosonde-measured winds are stronger. An immediate reduction in the wind speed bias was made by removing the semi-transparency corrections from irT. **Therefore, the first approach to a solution would be to re-evaluate the semi-transparency flags for mid-latitudes.**

The second factor, the influence of diffuse cloud on the water vapor measurements, needs to be investigated further. The water vapor-infrared regression uses the concept of opaque clouds at various atmospheric levels to model the cloud top temperature. Variation of temperature is assumed to be due to increasing number of optically thick clouds. The diffuse cloud top of an optically thick cloud cannot be explained by such a model, since the variation in wvT and irT is due to the structure of the boundary and not interference from the surface. A refinement of the conceptual model of opaque clouds for a diffuse cloud top seems necessary. Re-defining the underlying surface as a cloud may be useful.

The third factor, view geometry differences between METEOSAT and the nadir viewing AVHRR instrument, can also be explained by the concept of a diffuse cloud top. The large view angle of METEOSAT will result in the detection of the effective emitting level in the infrared at a higher altitude than the nadir viewing AVHRR. The tracked clouds, however, should have wind speeds independent of view geometry. This can be studied by looking at a latitude dependence and an off-nadir dependence (near the equator). Since the viewing geometry for MSG will be the same, it is important that this source of error be investigated further.

The new SEVIRI instrument on board the MSG satellite offers opportunities for improvements. An analysis environment, such as KLAROS, already uses some of the available SEVIRI channels, those of AVHRR, to estimate cloud properties, such as cloud top temperatures, emissivities, and in the future, phase. Similar channels of SEVIRI can lead to improvement of height assignment in the classification of cloud fields, phase determination, integration of cloud tracking and cloud properties, and higher spatial and temporal resolution. The only parameter which will not be improved with MSG is the viewing geometry. Since this has been linked as a possible cause to the bias, it is worth studying in more detail.

Acknowledgments

This project was funded by the EUMETSAT contract EUM/CO/00/354. We thank Ken Holmlund of EUMETSAT for providing the AMV database upon which this study is based. The authors wish to thank Dave Donovan, at KNMI, for help in creating the Delft radar images. We also would like to thank Niels Bormann, at ECMWF, for his helpful discussions and suggestions for this project. Copies of the complete final report are available upon request from the authors. Animations of the METEOSAT images can be found at *http://www.knmi.nl/~dlhopols/AAA/presentation.html*

References

Bormann, N. Characterizing and Correcting Speed Biases in Atmospheric Motion Vectors within the ECMWF Assimilation System. *EUMETSAT/ECMWF Fellowship Programme: First Year Report*, 2001.

Dlhopolsky, R. and Feijt, A., 2003: Representative Heights for Atmospheric Motion Vectors, EUMETSAT Final Report EUM/CO/00/354.

Feijt, A., ten Brink, H., Jongen, S., van Lammeran, A. and Russchenberg, H., 1999: Validation of Cloud Parameter Retrieval methods with objective ground based measurements. *Physical Chemistry of the Earth*, **24**, 173-176.

Gustafsson N., 1993: HIRLAM 2 Final Report. *SMHI Technical Report* 9., 129pp.

Holmlund, K. 1998: The Utilization of Statistical Properties of Satellite-Derived Atmospheric Motion Vectors to Derive Quality Indicators, *Weather and Forecasting*, 13, 1093-1104.

Liao, X., Rossow, W. B., Rind, D., 1995: Comparison between SAGE II and ISCCP high-level Clouds 2. Locating Cloud Tops, Journal of Geophysical Research, 100, 1137-1147.

Rao, C. R. N. and Chen, J., Post Launch calibration of the visible and near-infrared channels of the Advanced Very High Resolution Radiometer on the NOAA-14 Spacecraft,*International Journal of Remote Sensing*, 14, 2743-2747, 1996.

Saunders, R. W., Kriebel, K. T., An Improved Method for detecting clear sky and cloudy radiances from AVHRR data, *International Journal of Remote Sensing,* 9, 123-150, 1988.

Schmetz, J., Holmlund, K. Hoffman, J., Strauss, B., Mason, B., Gaertner, V., Koch, A. , van de Berg, L. : Operational Cloud-motion Winds from Meteosat Infrared Images, *Journal of Applied Meteorology*, 32, 1206-1225.

OVERZICHT VAN RECENT VERSCHENEN KNMI-PUBLICATIES / RECENTELY PUBLISHED AT KNMI

◄ KNMI-PUBLICATIE MET NUMMER / KNMI PUBLICATIONS (MISCELLANEOUS)

186-III Rainfall generator for the Rhine Basin: nearest-neighbour resampling of daily circulation indices and conditional generation of weather variables / Jules J. Beersma and T. Adri Buishand

186-IV Rainfall generator for the Rhine Basin: multi-site generation of weather variables for the entire drainage area / Rafal Wójcik, Jules J. Beersma and T. Adri Buishand

186-V Rainfall generator for the Rhine Basin: description of 1000-years simulations / Jules J. Beersma

191 Het KNMI-programma HISKLIM (HIStorisch KLIMaat) / T. Brandsma, F. Koek, H. Wallbrink en G. Können

192 Gang van zaken 1940-48 rond de 20.000 zoekgeraakte scheepsjournalen / Hendrik Wallbrink en Frits Koek

193 Science requirements document for OMI-EOS / contr. by R. van der A .. [et al.] **(limited distribution)**

194-1 De zonsverduistering van 11 augustus 1999, deel 1: de waarnemingen van het gedrag van flora en fauna / Jacob Kuiper, m.m.v. Guus Kauffeld

195 An optimal infrasound array at Apatity (Russian Federation) / Läslo Evers and Hein Haak **(limited distribution)**

196-I Rainfall Generator for the Meuse Basin: simulation of 6-hourly rainfall and temperature for the Ourthe catchment / Rafal Wójcik and T. Adri Buishand

197 Meteorologie op zee: beknopte handleiding voor waarnemingen op zee [= manual meteorology at sea] **(limited distribution)**

198 Projectie van de Elbe-zomerneerslag op de Rijn en Maas : onderzoek naar aanleiding van de recente overstromingen in Midden Europa / J.R.A. Onvlee en G.P. Können

199-I Droog, droger, droogst : bijdrage van het KNMI aan de eerste fase van de Droogtestudie Nederland / J.J. Beersma en T.A. Buishand

200 Aerosol Retrieval and Assimilation (ARIA) : final report / G.H.L. Verver, J.S. Henzing, G. de Leeuw, C. Robles-Gonzales and P.F.J. van Velthoven **(limited distribution)**

201 Sciamachy data assimilation 2 / J.F. Meirink, H.J. Eskes, M. van Weele and H.M. Kelder **(limited distribution)**

◄ PROCEEDINGS (PR) ISSN 1570-9345

2002-01 24th EWGLAM and 9th SRNWP meetings: 7-10 October 2002, KNMI, De Bilt / [edited by G. Cats]

◄ TECHNISCH RAPPORT = TECHNICAL REPORT (TR) ISSN 0169-1708

233 Vectorization of the ECBilt model / X. Wang and R.J. Haarsma

234 Evaluation of a plant physiological canopy conductance model in the ECMWF land surface scheme / J. van de Kassteele

235 Uncertainty in pyranometer and pyrheliometer measurements at KNMI in De Bilt / J.S. Henzing and W.H. Knap

236 Recalibration of GOME spectra for the purpose of ozone profile retrieval / Ronald van der A

237 Tracing water masses in the Atlantic / Yann Friocourt and Siebren Drijfhout

238 Klimaat voor Amsterdam Airport Schiphol / A. Smits

239 Seismische analyse van de aardbevingen bij Alkmaar op 9 en 10 september en Bergen aan Zee op 10 oktober 2001 / H.W. Haak, B. Dost en F.H. Goutbeek

240 EBEX-2000 : the KNMI/WAU contribution / W. Kohsiek, E.W. Meijer, P.J.B. Versteeg, O.K. Hartogensis, H.A.R. de Bruin

241 Ontwikkeling gidsvergelijkingen voor meerdaagse neerslagkansen / D. Vogelezang en K. Kok

242 On photosynthesis parameters for the A-gs surface scheme for high vegetation / G.J. Steeneveld

243 Temperatuurvergelijkingen voor de Middellange Termijn Gids : ontwikkeling en verificatie over 2000 / J.Wijngaard

244 Verification of clear-air turbulence forecasts / A. Overeem

245 A comprehensive description of the KNMI seismological instrumentation / B. Dost and H. Haak

246 Verandering van neerslagarakteristieken in Nederland gedurende de periode 1901-2001 / A.T.H. Bruin

247 Het nachtelijk uur en de kans op stralingsmist / J. Terpstra **(nog niet gepubliceerd / not yet published)**

248 BoWa NL: visie bovenluchtwaarnemingen Nederland / S. Tijm, B. Wichers Schreur en H. Klein Baltink

249 An investigation of the representative heights for atmospheric motion vectors / R. Dlhopolsky and A. Feijt

◄ WETENSCHAPPELIJK RAPPORT = SCIENTIFIC REPORT (WR) ISSN 0169-1651

01-03 Impact assessment of a doppler wind lidar in space on atmospheric analyses and numerical weather prediction / G.J. Marseille, A. Stoffelen, F. Bouttier, C. Cardinali, S. de Haan and D. Vasiljevic

02-01 Quality control and wind retrieval for SeaWinds / M. Potabella and A. Stoffelen

02-02 Shortwave radiation and cloud parameterizations for intermediate complexity models / J.J. Beersma, R. van Dorland and J.D. Opsteeg

02-03 Sensitivity study of the residue method for the detection of aerosols from space-borne sensors / M. de Graaf

02-04 Assimilation of satellite derived surface heating rates in a Numerical Weather Prediction model / Bart van den Hurk and Han The

02-05 On the use of physical and statistical downscaling techniques for NWP model output / Wim de Rooy and Kees Kok

02-06 ENVISAT Land Surface processes Phase 2 : final report / B.J.J.M. van den Hurk, Z. Su, W. Verhoef, G. Roerink and L. Jia

02-07 Effects of aerosols on UV-index / J. Badosa and M. van Weele

02-08 MERCI - Measurement error and correlation impact on the atmospheric dynamics mission / A. Stoffelen, P. Flamant, M. Hakansson, E. Källén, G.-J. Marseille, J. Pailleux, H. Schyberg amd M. Vaughan

02-09 Influence of clouds on the solar radiation budget / H.M. Deneke